

Article

Transmission Power Determination Based on Power Amplifier Operations in Large-Scale MIMO-OFDM Systems

Byung Moo Lee ¹ and Youngok Kim ^{2,*}

¹ School of Intelligent Mechatronics Engineering, Sejong University, Seoul 05006, Korea; blee@sejong.ac.kr

² Department of Electronic Engineering, Kwangwoon University, Seoul 01897, Korea

* Correspondence: kimyoungok@kw.ac.kr; Tel.: +82-2-940-5404

Academic Editor: Christos Bouras

Received: 29 April 2017; Accepted: 7 July 2017; Published: 9 July 2017

Abstract: This paper presents a method to determine transmission power based on power amplifier (PA) operations in order to improve the energy efficiency (EE) of a large-scale (LS) Multiple Input Multiple Output (MIMO)-OFDM system, which is a multi-carrier multiple antenna system with a large amount of transmitter (TX) antennas. Regarding the EE improvement, we propose two kinds of PA operation schemes: increasing the effective TX power (ITXP) and reducing the PA power consumption (RPC) assuming that a reduction of peak-to-average power ratio is applied in the appropriate manner. Closed-form expressions of relative EE are derived for both schemes, and the relative EE of the ITXP scheme is shown to depend on the precoding method that is applied to reduce the inter-user interference, while that of the RPC scheme is independent of the precoding method. The relative EE difference between the ITXP and the RPC schemes is also shown to rely on the occupation ratio of the PA power consumption over the total power consumption. Thus, the EE can remarkably improve by selecting the appropriate scheme based on the circumstances. The results of a simulation also validate the derived closed-form expression of the relative EE.

Keywords: antenna; large-scale MIMO; energy efficiency; power amplifier

1. Introduction

The ever increasing demand for high quality wireless services has resulted in an increase in the power consumption of wireless systems. Multiple Input Multiple Output (MIMO) is a key technology in a modern wireless communications, and it has already been adopted in the several standards, including 3GPP-LTE-Advanced, IEEE 802.11ac/ax, etc. In general, traditional point-to-point MIMO systems use almost the same number of transmitter (TX) and receiver (RX) antennas to maximize the channel capacity, and the 3GPP LTE-Advanced (Release 10, 11) incorporates a number of antennas up to 8 for a real implementation. If we can increase the number of antennas up to several hundred or more, we can obtain an enormous capacity gain. Recently, T. Marzetta suggested a MIMO system with several hundred TX antennas [1–5], which can be referred to as a large-scale (LS)-MIMO system. The basic form of LS-MIMO has been already discussed as a core technology for 5G systems. To realize a LS-MIMO system, however, many obstacles, such as the less correlated antenna implementation [6,7], the radio-frequency (RF) devices implementation [8,9], the reference signal overhead reduction [3], need to be overcome. LS-MIMO system has the potential to enhance the energy efficiency (EE), because it can generate an excessive amount of channel gain by using the massive antenna system [10]. However, many power amplifiers (PAs) are required for an LS-MIMO system because the signals radiated from each antenna need to be amplified by the PA, which is one of the most expensive and power hungry devices in the current base station (BS). Note that PA takes 50~80% of total power

consumption in current BS [11]. Therefore, the operation of PAs can be very important to improve the EE of an LS-MIMO system.

It is well-known that orthogonal frequency-division multiplexing (OFDM) is a very attractive modulation choice, and there is no doubt that it would be combined with LS-MIMO for efficient frequency usage. However, OFDM signal suffers from very high peak-to-average power ratio (PAPR) and current BS uses digital predistortion (DPD) technologies to compensate it [12]. Since DPD is an expensive device, it cannot be used for LS-MIMO due to the excessive amount of TX antennas, while there are numerous well-known PAPR reduction techniques and some can be successfully applied in LS-MIMO-OFDM to increase EE [13].

The LS-MIMO-OFDM can extend cell coverage due to its beamforming effect. However, the extension in coverage is not always beneficial in modern high data rate wireless communication systems because one BS needs to support more users under maintaining a high data transfer services in such a situation. In this paper, we show that both increasing the effective radiation power based on beamforming effect under maintaining the PA power consumption, and reducing the effective radiation power based on the degree of beamforming effect under reducing PA power consumption can increase EE significantly.

In the literature, several works focus on the transmission power and the related EE of LS-MIMO [14–18]. An optimization technique with various system parameters was used to find the global optimum point of the EE of LS-MIMO in [14]. In [15], an energy-efficient resource allocation problem was investigated for the downlink LS-MIMO frequency-division duplexing (FDD) system under a correlated Rayleigh fading channel. In this work, the authors tried to maximize the EE by adjusting the training duration, training power, and data power, under the constraints of a total transmit energy and spectral efficiency requirement for a user, which simultaneously evaluates the impact of the training and data transmission phases simultaneously. In [16], the authors derived tractable expressions for achievable uplink rate in a large-antenna limit, which approximates the results holding for any finite number of antennas. The results of analysis produced the scaling law that the users' transmit power should satisfy, while maintaining a desirable quality of service. In [17], an optimal resource allocation scheme, which jointly selects the training duration, the training signal power, and the data signal power maximizing the sum spectral efficiency for a given total energy budget spent in a coherence interval, was introduced. A closed-form approximation of the TX power based on an optimization scheme was also introduced in [18]. Even though all the previous works provide rather elegant schemes to improve the EE of an LS-MIMO, however, there is little work focusing on operating PA and relating the operation with the transmission power of the LS-MIMO-OFDM. This kind of work is very important from a practical point of view because the power control is based on the PA operation.

In this paper, we propose two PA operation schemes: increasing the effective TX power (ITXP) and reducing the PA power consumption (RPC), for the EE improvement in a LS-MIMO-OFDM system with a PAPR reduction technique. Unlike the resource allocation and/or optimization schemes for TX power, we focus on PA operation and connect its operation with TX power. Assuming that the PAPR reduction technique is applied in an appropriate way, depending on the situation, we can choose between two different PA operating modes to effectively improve the EE. The ITXP is the scheme that increases the TX power by maintaining the total power consumption as a constant, while the RPC is a scheme maintains the TX power as a constant by reducing the total power consumption. The closed-form expressions of relative EE for two schemes are derived, and the relative EE of the ITXP scheme is shown to depend on the performance of the precoding method which applied to reduce the inter-user interference (IUI), while that of the RPC scheme is independent of the precoding method. The result of a theoretical analysis and simulation show that the EE performance for both schemes is heavily dependent on the occupation ratio of the PA power consumption over the total power consumption.

In what follows, the system model and the proposed schemes are described in Section 2, and the closed-form expression of EE is derived in Section 3. An analysis of the performance and the results of simulation are presented in Section 4, and concluding remarks are given in Section 5.

2. System Model and Power Amplifier Operations

2.1. LS-MIMO-OFDM and PAPR

A single isolated cell with a BS using the LS-MIMO-OFDM system and K terminals is considered. The BS has N_t TX antennas, and each terminal has only one RX antenna. Let the frequency domain of an OFDM signal of the t -th antenna be $\mathbf{X}_t (= [X_t[0], X_t[1], \dots, X_t[N - 1]]^T)$. Then, the time domain signal \mathbf{x}_t can be represented as follows:

$$\mathbf{x}_t = \mathbf{F}_N^H \mathbf{X}_t, t = 1, \dots, N_t, \tag{1}$$

where \mathbf{F}_N^H is N -point IFFT matrix, which can be represented as $F_{n,k} = \frac{1}{\sqrt{N}} e^{-j2\pi nk/N}, 0 \leq n, k \leq N - 1$, and $x_t(n) = \frac{1}{\sqrt{N}} \sum_{k=0}^{N-1} X_t[k] e^{j2\pi nk/N}$.

To measure the PAPR of the OFDM signal, oversampling is usually considered to catch the PAPR of the analog domain. Note that most of the nonlinear distortions due to a high PAPR are caused in the analog domain, but most of the signal processes for the PAPR reduction are performed in the digital domain. The PAPR of the digital domain is not necessarily the same as the PAPR of the analog domain. However, 4-times of oversampling is well-known to be sufficient in satisfactorily approximating the PAPR of the analog domain [19]. If we consider the oversampled OFDM signal, (1) can be represented as follows:

$$\mathbf{x}_t^o = (\mathbf{F}^o)^H \mathbf{X}_t^o, t = 1, \dots, N_t, \tag{2}$$

where \mathbf{x}_t^o is the oversampled signal of \mathbf{x}_t , \mathbf{X}_t^o is the zero-padded signal of \mathbf{X}_t to generate the oversampled time domain signal, $(\mathbf{F}^o)^H$ is LN -point IFFT matrix, which can be represented as $F_{n,k}^o = \frac{1}{\sqrt{LN}} e^{-j2\pi nk/LN}, 0 \leq n, k \leq LN - 1$, and $x_t^o(n) = \frac{1}{\sqrt{LN}} \sum_{k=0}^{LN-1} X_t[k] e^{j2\pi nk/LN}$, and L is the oversampling factor.

Then, the PAPR of the OFDM signal for the t -th antenna can be expressed as follows:

$$PAPR = \frac{LN \cdot \|\mathbf{x}_t^o\|_\infty^2}{E[\|\mathbf{x}_t^o\|_2^2]}, \tag{3}$$

where $E[\cdot]$, $\|\mathbf{x}_t^o\|_\infty$, and $\|\mathbf{x}_t^o\|_2$ denote the expectation of $[\cdot]$, the l_∞ -norm, and l_2 -norm of vector \mathbf{x}_t^o , respectively. From now on, we omit the oversampling superscription for simplicity.

Cyclic prefix (CP) is necessary to remove the inter-symbol interference (ISI). If the CP is longer than the multipath delay spread, the individual frequency carrier experiences a flat fading channel, and the frequency domain representation of the received k th signal vector, $\mathbf{Y}[k] (= [Y_1[k], Y_2[k], \dots, Y_K[k]]^T)$, can be represented as follows:

$$\mathbf{Y}[k] = \sqrt{P_{tx}} \mathbf{H}[k] \mathbf{X}[k] + \mathbf{N}[k], \tag{4}$$

where $\mathbf{Y}[k]$ is the $K \times 1$ received vector for each terminal, P_{tx} is the total TX power for a forward link, $\mathbf{H}[k]$ is the $K \times N_t$ small scale i.i.d. Rayleigh fading channel matrix between N_t BS antennas and K terminals, $\mathbf{X}[k]$ is the $N_t \times 1$ signal vector for each antenna, and $\mathbf{N}[k]$ is the $K \times 1$ noise (AWGN) vector.

The precoding process is necessary to reduce the IUI, and there are two representative precoding schemes for the LS-MIMO: matched filtering (MF) and zero forcing (ZF) schemes [1]. Both schemes are considered in this paper, and the precoding matrices for MF and ZF are summarized in Table 1.

Table 1. The precoding matrices of MF and ZF.

Precoding	MF	ZF
\mathbf{W}	$N_t^{-1}\mathbf{H}^H$	$\mathbf{H}^H(\mathbf{H}\mathbf{H}^H)^{-1}$

Generally the performance of the ZF precoding scheme is known to be superior to that of the MF precoding scheme. However, the MF scheme is also known to be simple and effective especially when the number of TX antennas is very large. Moreover, the MF scheme is suitable for a distributed antenna system because each distributed antenna system does not need to know the channel information of the other antenna systems [1]. The signal transmitted after precoding, \mathbf{X} , can be represented as follows:

$$\mathbf{X} = \zeta \mathbf{W}\mathbf{S}, \tag{5}$$

where ζ is the TX power normalization factor, which is approximated as $\zeta = \frac{1}{\|\mathbf{W}\mathbf{S}\|_F} \approx \sqrt{\frac{N_t}{K}}$, $\|\cdot\|_F$ denotes the Frobenius norm, \mathbf{W} is the $N_t \times K$ precoding matrix to reduce the IUI, and \mathbf{S} is the $K \times 1$ message signal vector.

2.2. Energy Efficiency Model and Power Amplifier Operation

The energy efficiency is defined to measure the EE gain and is usually expressed as follows:

$$EE = R/P_{tot}, \tag{6}$$

where R is the achievable rate in bits per second, and P_{tot} is the reference total power for the derivation of EE. For simplicity, we divide the P_{tot} into two parts as

$$P_{tot} = P_{PA} + P_R, \tag{7}$$

where P_{PA} is the power consumption of the PA, and P_R is the power consumption of the remaining relevant components. It is appropriate to define P_{tot} as (7) because the P_{PA} consumes most of the power in the current BS.

When a Class B amplifier is used, the relationship between the TX power, P_{tx} , and P_{PA} can be expressed as follows [20,21]:

$$P_{tx} = \eta P_{PA}, \tag{8}$$

where η is the PA efficiency in percentage (%) and is defined as

$$\eta = \frac{\pi}{4p}, \tag{9}$$

where p is the square-root of the input back-off (IBO), \sqrt{IBO} . The η depends heavily on the PAPR of the OFDM signal, as shown in Figure 1, and the PAPR of the OFDM signal also depends on the system bandwidth and/or number of subcarriers [20,21]. According to the 3GPP LTE system parameters [22], we can choose the 20MHz bandwidth with 1200 subcarriers/2048 FFT size. With these parameters, the PAPR of the OFDM signal is around 12dB from the complementary cumulative distribution function (CCDF = 10^{-3}) [23].

Now let us describe how (8) can be changed for the ITXP and the RPC schemes. First, we define the reference TX power for the case in which PAPR reduction technique is not applied, and it is expressed as follows:

$$P_{tx}^{ref} = \eta^{ref} P_{PA}^{ref}. \tag{10}$$

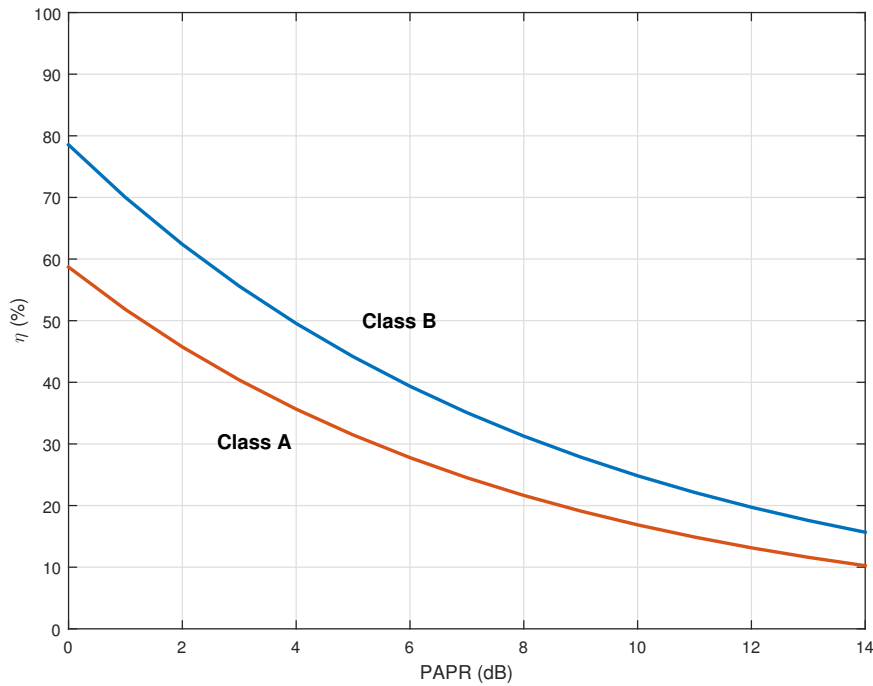


Figure 1. PA efficiency, η (%) versus PAPR(dB).

When the PAPR reduction technique and the ITXP scheme are applied, (10) can be rewritten as follows:

$$P_{tx}^{ITXP} = \eta^{PAPR} P_{PA}^{ref}, \tag{11}$$

where P_{tx}^{ITXP} is the TX power with the ITXP scheme, and η^{PAPR} is the PA efficiency after PAPR reduction. (11) means that η^{ref} increased to η^{PAPR} as a result of the PAPR reduction technique, while P_{PA}^{ref} is kept as is. That is, $P_{tx}^{ITXP} > P_{tx}^{ref}$, due to the increase in PA efficiency.

When the PAPR reduction technique and the RPC scheme are applied, (10) can be rewritten as follows:

$$P_{tx}^{RPC} = \eta^{PAPR} P_{PA}^{RPC}, \tag{12}$$

where P_{tx}^{RPC} is the TX power and P_{PA}^{RPC} is the PA power consumption with the RPC scheme. (12) means that η^{ref} increases to η^{PAPR} due to the PAPR reduction technique, while reducing PA power consumption from P_{PA}^{ref} to P_{PA}^{RPC} , and maintaining TX power. To make $P_{tx}^{RPC} = P_{tx}^{ref}$, we should choose $P_{PA}^{RPC} = \frac{P_{PA}^{ref}}{\eta^{PAPR}}$, and then, from (12), P_{tx}^{RPC} can be represented as follows:

$$\begin{aligned} P_{tx}^{RPC} &= \eta^{PAPR} \frac{P_{PA}^{ref}}{\eta^{PAPR}} \\ &= P_{tx}^{ref}. \end{aligned} \tag{13}$$

That is, by employing the RPC scheme, P_{tx}^{RPC} becomes equal to P_{tx}^{ref} , because of the increase in the PA efficiency η and reduction in the PA power consumption P_{PA} .

For easy understanding, we present Table 2 for the transmission powers of each scheme.

Table 2. Transmission Power for Each Scheme.

Reference	ITXP	RPC
$P_{tx}^{ref} = \eta^{ref} P_{PA}^{ref}$	$P_{tx}^{ITXP} = \eta^{PAPR} P_{tx}^{ref}$	$P_{tx}^{RPC} = \eta^{PAPR} P_{PA}^{RPC}$

3. Closed-Form of Relative Energy Efficiency Based on Channel Hardening Effect

In this section, the closed form expression of the energy efficiency is derived in the presence of the channel hardening effect.

The frequency domain expression of the k -th subcarrier signal received by the i -th user, $Y_i[k]$, is written as follows:

$$\begin{aligned}
 Y_i[k] &= \sqrt{P_{tx}} \mathbf{H}_{i,:}[k] \zeta \mathbf{W}_{:,i}[k] S_i[k] \\
 &+ \sqrt{P_{tx}} \sum_{l \neq i} \mathbf{H}_{i,:}[k] \zeta \mathbf{W}_{:,l}[k] S_l[k] \\
 &+ N_i[k],
 \end{aligned} \tag{14}$$

where $\mathbf{H}_{i,:}[k]$ is the $1 \times N_t$ channel vector of the k th subcarrier for the i th user, ζ is the TX power normalization factor ($\zeta \approx \sqrt{\frac{N_t}{K}}$) as mentioned in Section 2.1, $\mathbf{W}_{:,i}[k]$ is the $N_t \times 1$ precoding vector of k -th subcarrier for i th user, S_i is the k -th subcarrier message signal for i th user, and $N_i[k]$ is the k th subcarrier AWGN for i th user. The second line of (14) is the IUI term.

From (14), the effective SINR, γ_k , can be represented as follows:

$$\gamma_k[k] = \frac{\frac{P_{tx} N_t}{K} |\mathbf{H}_{i,:}[k] \mathbf{W}_{:,i}[k]|^2}{\frac{P_{tx} N_t}{K} \sum_{l \neq i} |\mathbf{H}_{i,:}[k] \mathbf{W}_{:,l}[k]|^2 + N_0 B}, \tag{15}$$

where $N_0 B$ is the noise power in a given bandwidth B .

Then, the achievable rate of the precoded LS-MIMO can be represented as follows:

$$R = \delta B \cdot \sum_{i=1}^K E \left[\log_2 \left(1 + \frac{\frac{P_{tx} N_t}{K} |\mathbf{H}_{i,:}[k] \mathbf{W}_{:,i}[k]|^2}{\frac{P_{tx} N_t}{K} \sum_{l \neq i} |\mathbf{H}_{i,:}[k] \mathbf{W}_{:,l}[k]|^2 + N_0 B} \right) \right], \tag{16}$$

where δ is the scaling factor for the pilot overhead and guard interval.

Since we deal with LS-MIMO, which has many TX antennas, an excessive amount of diversity gain can be obtained, and thus the channel hardening effect can happen and the randomness of the channel can be reduced.

In the presence of the channel hardening effect, (16) can be simplified by using the precoding matrix in Table 1 as follows [23]:

$$R_{approx}^{LS-MIMO} \approx \delta B K \cdot \left[\log_2 \left(1 + \frac{P_{tx} N_t}{(I + N_0 B) K} \right) \right], \tag{17}$$

where I is the IUI term. Note that the typical condition for (17) is $N_t \geq 10K$. By plugging (17) into (6), (6) can be rewritten as follows:

$$EE \approx \frac{\delta B K}{P_{PA} + P_R} \cdot \left[\log_2 \left(1 + \frac{\eta P_{PA} N_t}{(I + N_0 B) K} \right) \right]. \tag{18}$$

To better understand the characteristics of the EE and R, we present the simulation results for the relationship between the normalized EE versus P_{tot} and normalized R versus P_{tot} in Figure 2. The normalized EE and R mean the normalized values by the value of EE and R when $P_{tot} = 10$ each. As P_{tot} increases, the normalized R increases logarithmically, while the normalized EE increases only to a certain point and then decreases.

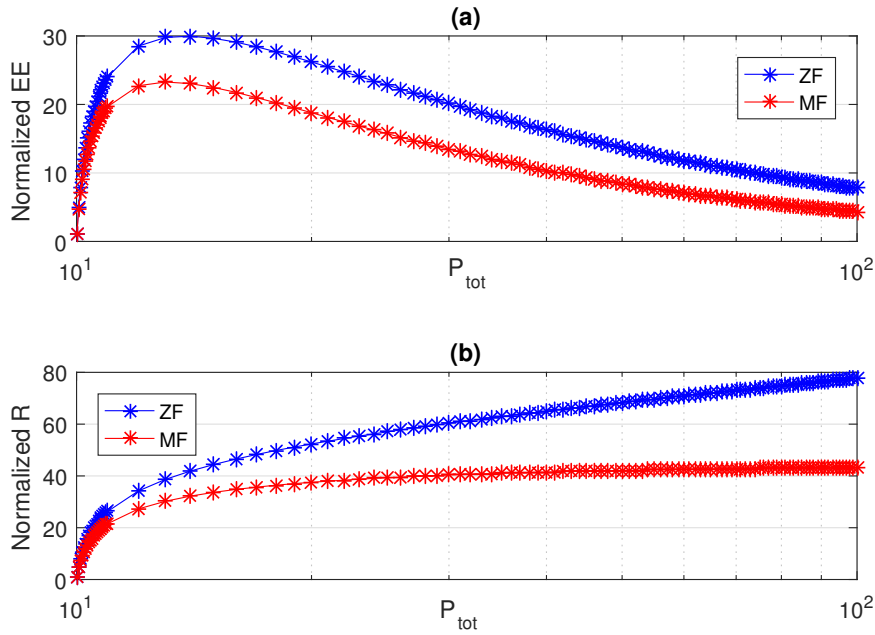


Figure 2. (a) Normalized EE versus P_{tot} ; (b) Normalized R versus P_{tot} , when $N_t = 400, K = 40$.

4. Performance Analysis and Simulation Results

In this section, we show the performance analysis and the related simulation results on the methodology of the PA operation.

4.1. Improvement of the Energy Efficiency

In this subsection, we analyze the EE performance based on the PAPR reduction. When PAPR reduction techniques are employed [13], we can secure a room to increase the energy efficiency. As mentioned in the previous sections, two strategies to improve the EE, which are the ITXP and RPC schemes, can be applied.

4.1.1. ITXP Scheme

From (11), the reduction of the PAPR is shown to increase the efficiency, η and it can consequently increase P_{tx} . Therefore, the ITXP scheme can increase the achievable rate and the EE by increasing the TX power. To show the improvement in EE, the relative EE with ITXP scheme, EE_r^{ITXP} is defined as the ratio of EE^{ITXP} and EE_{ref} . Note that EE_{ref} is the reference EE without PAPR reduction technique. The relative EE of ITXP is expressed as follows:

$$\begin{aligned}
 EE_r^{ITXP} &= EE^{ITXP} / EE_{ref} \\
 &\approx \frac{\frac{\delta BK}{P_{PA}^{ref} + P_R} \cdot \left[\log_2 \left(1 + \frac{\eta P_{PA}^{ref} N_t}{(I + N_0 B) K} \right) \right]}{\frac{\delta BK}{P_{PA}^{ref} + P_R} \cdot \left[\log_2 \left(1 + \frac{\eta^{ref} P_{PA}^{ref} N_t}{(I + N_0 B) K} \right) \right]} \\
 &= \frac{\left[\log_2 \left(1 + \frac{\eta^{PAPR} P_{PA}^{ref} N_t}{(I + N_0 B) K} \right) \right]}{\left[\log_2 \left(1 + \frac{\eta^{ref} P_{PA}^{ref} N_t}{(I + N_0 B) K} \right) \right]}, \tag{19}
 \end{aligned}$$

where η^{ref} is the reference PA efficiency, when no PAPR reduction technique is applied. Only the log terms of numerator and denominator remain, and as the PAPR reduction increases, the EE_r^{ITXP} also

increases. Since the IUI depends on the precoding method, the EE_r^{ITXP} can change with the applied precoding method.

4.1.2. RPC Scheme

As shown in (12), if the PAPR reduction technique is applied, η can increase. If we decide to fix the transmission power P_{tx}^{ref} , we can reduce the PA power consumption to $P_{PA}^{RPC} = \frac{P_{PA}^{ref}}{\eta^{PAPR}}$ by reducing the supply voltage of PA. When the RPC scheme is applied, therefore, the relative EE with RPC scheme, EE_r^{RPC} can be expressed as follows:

$$\begin{aligned}
 EE_r^{RPC} &= EE^{RPC} / EE_{ref} \\
 &\approx \frac{\frac{\delta BK}{\frac{P_{tx}^{ref}}{\eta^{PAPR}} + P_R} \cdot \left[\log_2 \left(1 + \frac{P_{tx}^{ref} N_t}{(I + N_0 B) K} \right) \right]}{\frac{\delta BK}{\frac{P_{tx}^{ref}}{\eta^{ref}} + P_R} \cdot \left[\log_2 \left(1 + \frac{P_{tx}^{ref} N_t}{(I + N_0 B) K} \right) \right]} \\
 &= \frac{\frac{P_{tx}^{ref}}{\eta^{ref}} + P_R}{\frac{P_{tx}^{ref}}{\eta^{PAPR}} + P_R} \\
 &= \frac{\eta^{PAPR} (P_{tx}^{ref} + \eta_{ref} P_R)}{\eta_{ref} (P_{tx}^{ref} + \eta^{PAPR} P_R)}.
 \end{aligned} \tag{20}$$

In contrast with the case of ITXP, in the case of RPC, the log terms are cancelled. Note that the relative EE with RPC scheme is independent of the precoding methods.

4.2. Performance Evaluation and Discussion

In this subsection, the performance of the both ITXP and RPC schemes is evaluated, and the decision criterion for the schemes is discussed.

For better understanding of this section, we present the channel hardening in Figure 3. The x -axis of the figure represents the ordered eigenvalue of $\mathbf{H}\mathbf{H}^H$, which converges to N_t , and y -axis represents the cumulative distribution function (CDF). Figure 3 shows the case in which the number of users is fixed to $K = 4$, and the number of TX antennas increases as $N_t = 4, 40,$ and 400 . As N_t increases, the randomness of the channel reduces.

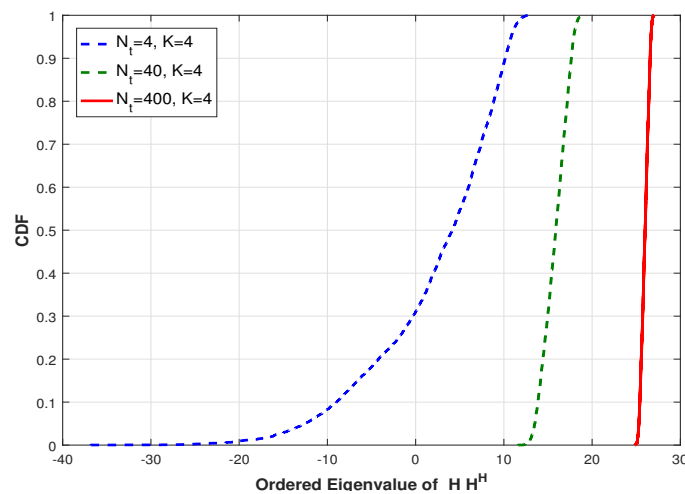


Figure 3. Channel hardening effect, when $N_t = 4, 40, 400$ and $K = 4$.

Then, we should consider the occupancy ratio of P_{PA} over P_{tot} . When P_{PA} takes a greater portion than P_R in the P_{tot} , a greater improvement in EE can be obviously achieved by using the IXP/RPC schemes. The PA is the most power hungry device, and takes 50~80% of the total power consumption, as we mentioned in Section 1. However, when the proposed schemes are applied in the LS-MIMO-OFDM, it is easily expected that the occupancy ratio of the P_{PA} could be significantly reduced, because the LS-MIMO system uses a large amount of TX antennas, and a beamforming effect can occur which allows a small radiation power and/or power consumption.

A discussion of the case with each scheme is followed by simulation and analytical results in Figure 4. Figure 4a shows the performance of the relative EE in terms of the PAPR reduction, when the PA power consumption takes 80% of the total power consumption, i.e., $P_{PA}:P_R = 80:20$. Since the RPC is independent of the precoding method, only one curve is shown for the RPC, while there are two curves for the IXP, ZF and MF because the relative EE of the IXP depends on the precoding method. In the figure, solid lines represent the results of the analysis of a previous subsection (Equations (19) and (20)), and the red/blue marks of '+'s indicate the results of the simulations. For the simulation, we use the i.i.d. Rayleigh fading channel with static/nomadic users based on Equation (16). For the analytical results, we use the derived closed-form equations, (17) and (18). Since the operating point of the system is in the LS-MIMO region ($N_t \geq 10 K$), due to the channel hardening effect, the analytical results are well-matched with the results of the simulations.

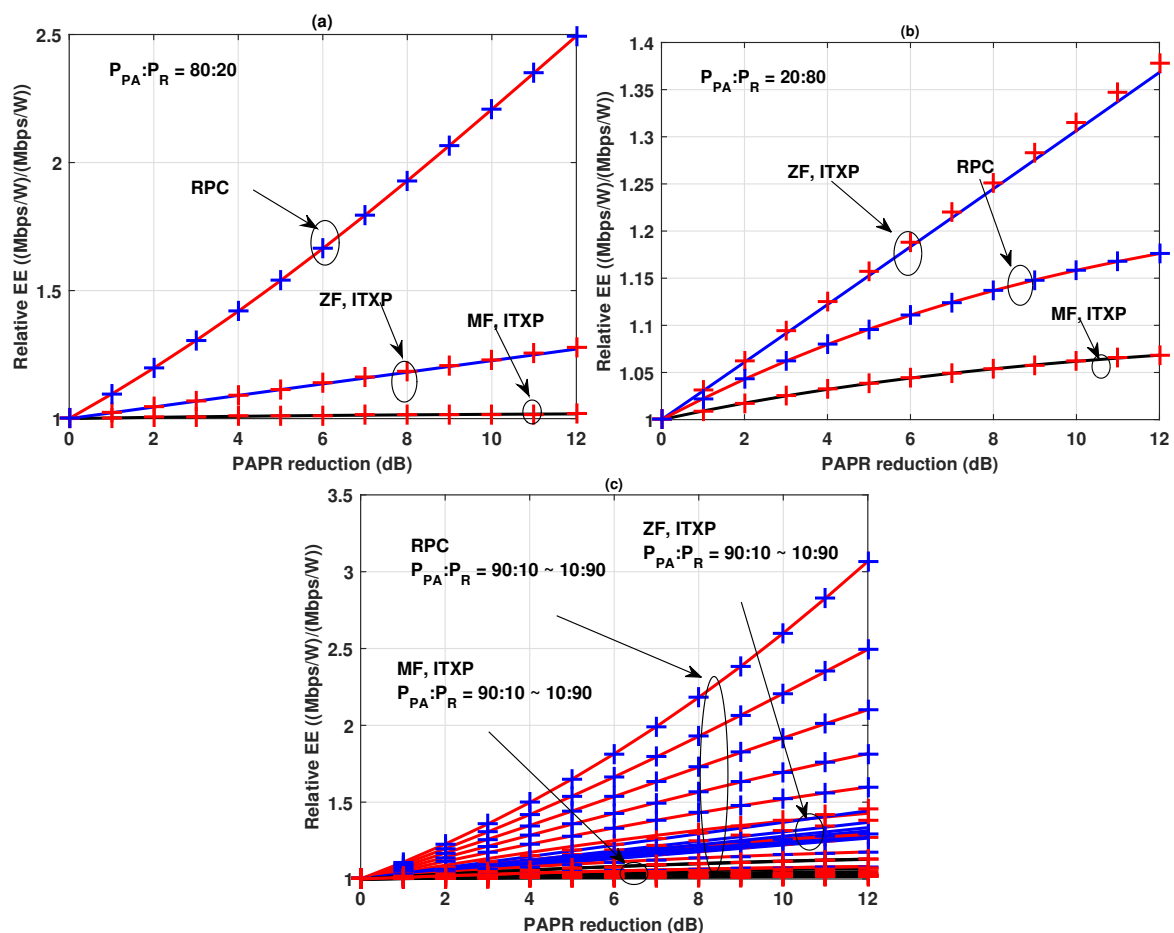


Figure 4. Relative EE versus PAPR reduction (dB), when $N_t = 400$, $K = 40$; (a) $P_{PA}:P_R = 80:20$; (b) $P_{PA}:P_R = 20:80$; (c) $P_{PA}:P_R = 90:10 \sim 10:90$. Solid lines represent the results of analysis (Equations (19) and (20)), and red/blue marks of '+'s indicate the results of simulations.

In the case of the MF, the ITXP scheme gives only a slight improvement because the increase in P_{tx} also causes an increase in interference. Although the ZF is superior to the MF in the ITXP scheme, the RPC scheme outperforms the ITXP scheme for both precoding methods.

However, this is not always true, as shown in Figure 4b. When the power consumption of the PA takes a much smaller portion, i.e., $P_{PA}:P_R = 20:80$, as shown in the figure, the ITXP scheme with ZF precoding outperforms the RPC scheme. We should keep in mind that the LS-MIMO system requires only a small TX power and this could induce a small P_{PA} and/or very large P_R because the RF components must be applied in each antenna which means that as the number of TX antennas increases, P_R can increase.

Therefore, for the LS-MIMO systems, we should consider both the ITXP and RPC schemes. Figure 4c shows the performance of relative EE in terms of the PAPR reduction when the ratio varies as follows: $P_{PA}:P_R = 90:10 \sim 10:90$.

It is obvious that when P_{PA} takes a larger portion, we can get a greater EE gain. Note that the analysis presented is based on the assumption that a good PAPR reduction technique is available, and a lot of related studies are going on [24].

To find the optimum operating strategy between two schemes, we define the threshold value, J as follows:

$$J = EE_r^{RPC} - EE_r^{ITXP} \tag{21}$$

When $J \geq 0$, we can choose the RPC. Otherwise we can choose ITXP for the optimum operation. Figure 5 present J versus P_{PA} , and the cross over point is not so much different even though we increase the P_{PA} .

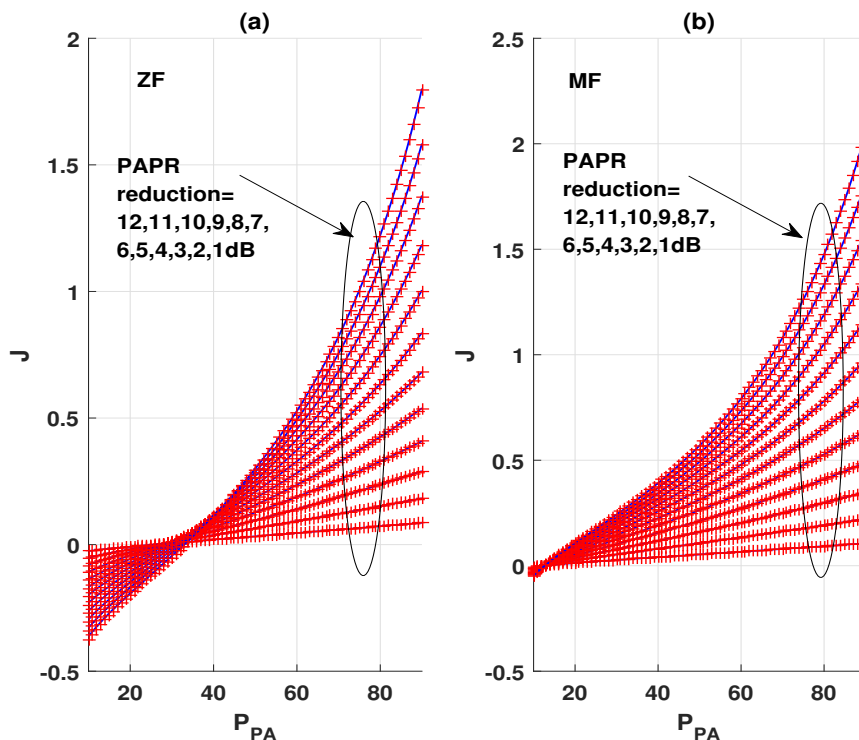


Figure 5. J versus P_{PA} , (a) ZF precoding, (b) MF precoding, when $N_t = 400, K = 40$. Lines are based on analysis from Equations (19) and (20), and red '+'s are simulation results.

In Table 3, we present points of the $J = 0$.

Table 3. $J = 0$ points for ZF and MF precoding.

PA Power Consumption	ZF	MF
P_{PA}	25.5~32.9	12.52~12.74

In the case of ZF precoding, if P_{PA} takes more than 25.5~32.9 when $P_{tot} = 100$, we should choose RPC, otherwise we should choose ITXP for the optimum EE operation. In the case of the MF precoding, if P_{PA} takes more than 12.52~12.74 when $P_{tot} = 100$, we should choose RPC, otherwise we should choose ITXP for the optimum EE operation. For example, when $P_{PA} = 33$ with a PAPR reduction =12 dB and ZF precoding, it is better to choose PRC because $J > 0$ at that point. The difference of $J = 0$ points among various PAPR reduction is not so significant, especially in the case of MF precoding. Also, in the case of MF precoding, P_{PA} for $J = 0$ points is smaller than that in the case of ZF precoding due to the fact that ITXP does not improve so much compared to the EE performance of the MF precoding relative to that of the ZF precoding because the interference also increases as the TX power increases. Since the analytical results are well-matched with the results of simulation, we can use the analytical results for J to determine the EE optimized operational scheme.

To show the characteristic of the decision threshold, J , we present three 3D graphs in Figure 6. As observed in Figure 6a, as P_{PA} and/or PAPR reduction increases, J also increases. It is also noteworthy that the proposed method is not affected by the variations in the parameters. As we can see from (b) and (c) of Figure 6, even though N_t and K change, the thresholds do not change.

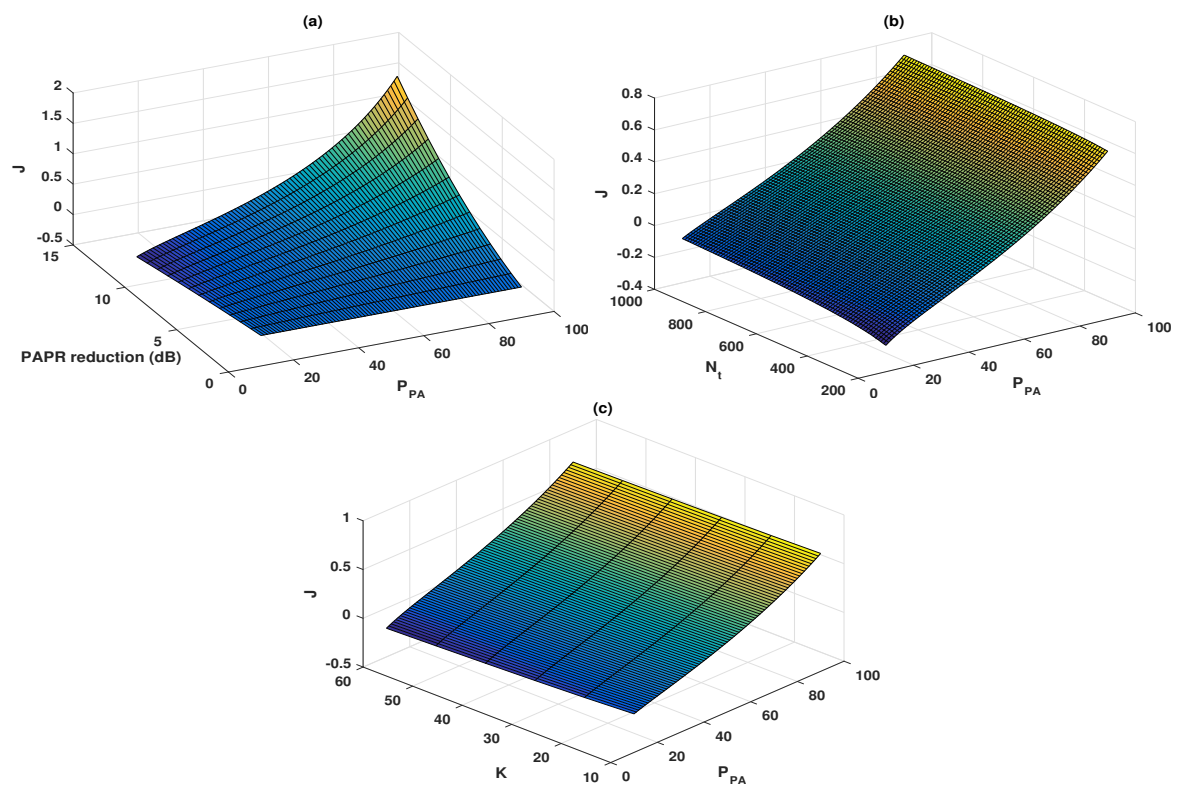


Figure 6. When $N_t = 400$, $K = 40$, (a) J versus PAPR reduction (dB) and P_{PA} ; (b) J versus N_t and P_{PA} ; (c) J versus K and P_{PA} .

5. Conclusions

The TX power determined based on the PA operations is discussed for the EE improvement of the LS-MIMO-OFDM system, and two PA operation schemes are proposed. The closed form of the expressions for the relative EE are derived for the schemes, and the performance of the proposed

schemes is evaluated with the corresponding simulations. According to a theoretical analysis and results of the simulation, the RPC scheme generally outperforms the ITXP scheme. However, the ITXP must also be considered coincidentally because the ITXP can outperform the RPC, especially when PA takes a small portion in the total power consumption. The ZF is also shown to provide enhanced EE performance compared to the MF, when the ITXP scheme is used.

Acknowledgments: This work was supported by the National Research Foundation of Korea (NRF) grant funded by the Korea government (Ministry of Education) (NRF-2017R1D1A1B03028350), and faculty research fund of Sejong University in 2017. This work was conducted by the research Grant of Kwangwoon University in 2017.

Author Contributions: Byung Moo Lee designed the algorithm, performed the simulations, and prepared the manuscript. Youngok Kim was responsible for coordinating, writing, and revising the paper. Both authors discussed the results and approved the publication.

Conflicts of Interest: The authors declare no conflict of interest.

References

1. Marzetta, T.L. Noncooperative Cellular Wireless with Unlimited Numbers of Base Station Antennas. *IEEE Trans. Wirel. Commun.* **2010**, *9*, 3590–3600.
2. Jabbar, S.Q.; Li, Y. Analysis and Evaluation of Performance Gains and Tradeoffs for Massive MIMO Systems. *Appl. Sci.* **2016**, *6*, 268, doi:10.3390/app6100268.
3. Lee, B.M.; Kim, Y. Beam Grouping Based RS Resource Reuse and De-Contamination in Large Scale MIMO Systems. *Appl. Sci.* **2017**, *7*, 96, doi:10.3390/app7010096.
4. Marzetta, T.L. Massive MIMO: An Introduction. *Bell Labs Tech. J.* **2015**, *20*, 11–22.
5. Björnson, E.; Larsson, E.G.; Marzetta, T.L. Massive MIMO: Ten myths and one critical question. *IEEE Commun. Mag.* **2016**, *54*, 114–123.
6. Guariglia, E. Entropy and Fractal Antennas. *Entropy* **2016**, *18*, 84.
7. Krzysztofik, W.J. Fractal Geometry in Electromagnetics Applications—From Antenna to Metamaterials. *Microw. Rev.* **2013**, *19*, 3–14.
8. Liu, A.; Lau, V. Phase Only RF Precoding for Massive MIMO Systems with Limited RF Chains. *IEEE Trans. Signal Process.* **2014**, *62*, 4505–4515.
9. Lee, B.M.; Kim, Y. Design of an Energy Efficient Future Base Station with Large-Scale Antenna System. *Energies* **2016**, *9*, 1083, doi:10.3390/en9121083.
10. Yang, H.; Marzetta, T.L. Energy Efficient Design of Massive MIMO: How Many Antennas? In Proceedings of the IEEE 81st Vehicular Technology Conference (VTC Spring), Glasgow, UK, 11–14 May 2015; pp. 1–5.
11. Wu, J.; Zhang, Y.; Zukerman, M.; Yung, E.K.N. Energy-efficient base-stations sleep-mode techniques in green cellular networks: A survey. *IEEE Commun. Surv. Tutor.* **2015**, *17*, 803–826.
12. Liu, Y.; Quan, X.; Shao, W.P.S.; Tang, Y. Performance Analysis of Direct-Learning Digital Predistortion with Loop Delay Mismatch in Wideband Transmitters. *IEEE Trans. Veh. Technol.* **2016**, *65*, 7078–7089.
13. Jiang, T.; Wu, Y. An Overview: Peak-to-Average Power Ratio Reduction Techniques for OFDM Signals. *IEEE Trans. Broadcast.* **2008**, *54*, 257–268.
14. Bjornson, E.; Sanguinetti, L.; Hoydis, J.; Debbah, M. Optimal Design of Energy-Efficient Multi-User MIMO Systems: Is Massive MIMO the Answer? *IEEE Trans. Wirel. Commun.* **2015**, *14*, 3059–3075.
15. Wang, Y.; Li, C.; Huang, Y.; Wang, D.; Ban, T.; Yang, L. Energy-Efficient Optimization for Downlink Massive MIMO FDD Systems with Transmit-Side Channel Correlation. *IEEE Trans. Veh. Technol.* **2016**, *65*, 7228–7243.
16. Zhang, Q.; Jin, S.; Wong, K.-K.; Zhu, H.; Matthaiou, M. Power Scaling of Uplink Massive MIMO Systems with Arbitrary-Rank Channel Means. *IEEE J. Sel. Top. Signal Process.* **2014**, *8*, 966–981.
17. Ngo, H.Q.; Matthaiou, M.; Larsson, E.G. Massive MIMO with Optimal Power and Training Duration Allocation. *IEEE Commun. Lett.* **2014**, *3*, 605–608.
18. Lee, B.M.; Kim, Y. Optimal transmission power determination to increase energy efficiency of large-scale MIMO antenna systems. *J. Electromagn. Waves Appl.* **2017**, *31*, 383–393.
19. O’Neil, R.; Lopes, L.N. Envelop variations and spectral splatter in clipped multicarrier signals. In Proceedings of the 6th IEEE International Symposium on Personal, Indoor and Mobile Radio Communications (PIMRC ’95), Toronto, ON, Canada, 27–29 September 1995; Volume 1, pp. 71–75.

20. Wulich, D. Definition of Efficient PAPR in OFDM. *IEEE Commun. Lett.* **2005**, *9*, 832–834.
21. Cripps, S.C. *RF Power Amplifiers for Wireless Communications*, 2nd ed.; Artech House: Norwood, MA, USA, 2006.
22. Sesia, S.; Toufik, I.; Baker, M. *LTE, The UMTS Long Term Evolution: From Theory to Practice*; Wiley: Chichester, UK, 2009.
23. Lee, B.M.; Choi, J.H.; Bang, J.H.; Kang, B.C. An energy efficient antenna selection for large scale green MIMO systems. In Proceedings of the 2013 IEEE International Symposium on Circuits and Systems (ISCAS), Beijing, China, 19–23 May 2013; pp. 950–953.
24. Studer, C.; Larsson, E.G. PAR-Aware Large-Scale Multi-User MIMO-OFDM Downlink. *IEEE J. Sel. Areas Commun.* **2013**, *31*, 303–313.



© 2017 by the authors. Licensee MDPI, Basel, Switzerland. This article is an open access article distributed under the terms and conditions of the Creative Commons Attribution (CC BY) license (<http://creativecommons.org/licenses/by/4.0/>).